Intensity and Distribution of Hybrid-Mode Fields in Dielectric-Loaded Waveguides

KAWTHAR A. ZAKI, SENIOR MEMBER, IEEE, AND CHUNMING CHEN, STUDENT MEMBER, IEEE

Abstract — **Plots of the intensity and distribution of the electric and magnetic fields of several propagating and evanescent hybrid modes in dielectric-loaded circular waveguides are derived and presented. These plots have not been reported in the literature before, and can be very valuable in applications using dielectric-loaded waveguides and resonators, including microwave, millimeter-wave, and optical guiding structures.**

I. Introduction

ANALYSIS METHODS for the determination of the electromagnetic fields in dielectric-loaded waveguides and cavity resonators have recently received considerable attention. Among the methods being developed are techniques based on field expansions in terms of eigenmodes of the guiding structure, the resonators and enclosures [1]–[5], and on surface integral equations [6]. The results of these approaches provide quantitative design information that can help in the development of new microwave and millimeter-wave components.

Pictorial display of the transverse fields of various hybrid modes in the cross section of a dielectric-loaded waveguide (Fig. 1) gives significant insight about the field structure. Such a display can help in the design of devices using these modes by indicating the locations of strong fields, their directions, etc., so that this information can be used to decide the locations of tuning obstacles to adjust the resonant frequencies of cavities, coupling irises or probes to excite these modes, or discontinuities to suppress or avoid the excitation of spurious modes. Kobayashi and Tanaka [3] calculated the field patterns for hybrid modes for the case of a dielectric rod without an exterior boundary. They presented the field patterns only inside the dielectric rod, except for the HE_{11} mode, where portions of the fields outside the dielectric were displayed. Recently, Moller and Macphie [7] presented sequences of field plots illustrating the time-varying behavior of fields near discontinuities in waveguides. The purpose of this paper is to present 1) a method for the numerical computation and plotting of the electromagnetic field distribution in a dielectric loaded waveguide, and 2) the results of the computations showing the intensity of the electric and magnetic fields as well as the field lines for various modes that could exist in the structure.

Manuscript received March 15, 1985; revised May 26, 1985. This material is based upon work supported by the National Science Foundation under Grant ECS-8320249.

The authors are with the Department of Electrical Engineering, University of Maryland, College Park, MD 20742.

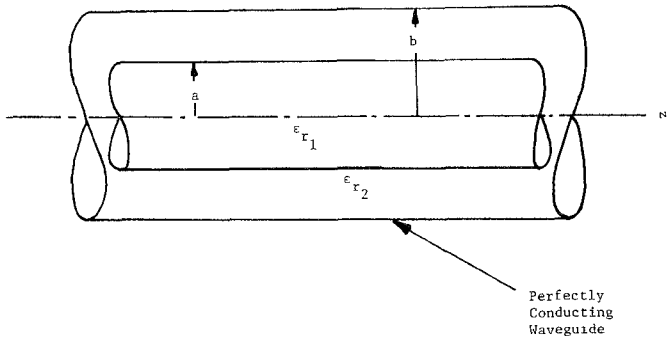

Fig. 1. Dielectric-loaded waveguide.

II. Method of Field Plotting[1]

The electric (or magnetic) field lines are solutions of the first-order differential equation [8]

$$\frac{dy}{dx} = \tan[\alpha(x, y)] = \frac{E_y(x, y)}{E_x(x, y)} \tag{1}$$

where α is the angle between the field vector at (x, y) and the positive x-axis. The Cartesian field components E_x and E_y are expressible in terms of the polar components E_r and E_ϕ by (see Fig. 2)

$$E_x = E_r \cos\phi - E_\phi \sin\phi \tag{2}$$

$$E_y = E_r \sin\phi + E_\phi \cos\phi. \tag{3}$$

A first-order numerical approximation to that trajectory passing through a point P_i is shown in Fig. 2. The calculations of the trajectory are made by using a first-order difference scheme in which the point P_{i+1}, whose coordinates are (x_{i+1}, y_{i+1}), is determined from the point P_i, whose coordinates are (x_i, y_i), according to the relations

$$x_{i+1} = x_i + \delta s \cos\alpha_i \tag{4}$$

$$y_{i+1} = y_i + \delta s \sin\alpha_i \tag{5}$$

where δs is a selected path increment.

For the numerical determination of the field lines, several points need to be taken into account to ensure their accurate plotting. First, the choice of the path increment should be made sufficiently small to give smooth and accurate contour lines, yet not too small to necessitate undue amounts of calculations. Second, the starting (or

[1]Although the discussion in this section is presented using electric field components, the same process applies for the magnetic field.

0018-9480/85/1200-1442$01.00 ©1985 IEEE

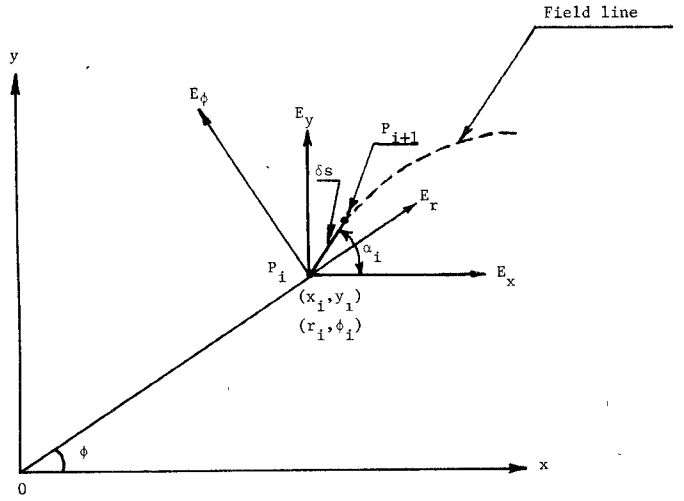

Fig. 2. First-order difference solution for the field lines.

boundary) points of the contours should be chosen such that the contour lines may not always be coincident with the boundary. Finally, each of the field components E_r and E_ϕ in (2) and (3) are expressible as the product of two functions: one is a function of r only, while the other is a function of ϕ only [1], i.e.,

$$E_r = e_r(r)\cos n\phi, \quad H_r = h_r(r)\sin n\phi \tag{6}$$

$$E_\phi = e_\phi(r)\sin n\phi, \quad H_\phi = h_\phi(r)\cos n\phi. \tag{7}$$

The functions $e_r(r)$ and $e_\phi(r)$ (and $h_r(r)$ and $h_\phi(r)$ for the magnetic field) are given by [1]

$$e_r(r) = -\frac{A\gamma}{\xi_1^2}\left[\xi_1 J_n'(\xi_1 r) + \frac{\alpha n J_n(\xi_1 r)}{r}\right], \quad 0 \leqslant r < a$$

$$= \frac{A\gamma}{\zeta_2^2}\left[\zeta_2 R_n'(\zeta_2 r) + \alpha n \frac{P_n(\zeta_2 r)}{r}\right], \quad a \leqslant r \leqslant b \tag{8a}$$

$$e_\phi(r) = \frac{A\gamma}{\xi_1^2}\left[\frac{nJ_n(\xi_1 r)}{r} + \alpha\xi_1 J_n'(\xi_1 r)\right], \quad 0 \leqslant r \leqslant a$$

$$= \frac{A\gamma}{\zeta_2^2}\left[\frac{nR_n(\zeta_2 r)}{r} + \alpha\zeta_2 P_n'(\zeta_2 r)\right], \quad a \leqslant r \leqslant b \tag{8b}$$

$$j\omega\mu h_r = \frac{A}{\xi_1^2}\left[\frac{nk_1^2 J_n(\xi_1 r)}{r} - \alpha\gamma^2\xi_1 J_n'(\xi_1 r)\right], \quad 0 \leqslant r \leqslant a$$

$$= -\frac{A}{\zeta_2^2}\left[\frac{nk_2^2 R_n(\zeta_2 r)}{r} - \alpha\gamma^2\zeta_2 P_n'(\zeta_2 r)\right], \quad a \leqslant r \leqslant b \tag{8c}$$

$$j\omega\mu h_\phi = -\frac{A}{\xi_1^2}\left[-k_1^2\xi_1 J_n'(\xi_1 r) + \frac{\alpha\gamma^2 n J_n(\xi_1 r)}{r}\right], \quad 0 \leqslant r \leqslant a$$

$$= \frac{A}{\zeta_2^2}\left[-k^2\zeta_2 R_n'(\zeta_2 r) + \frac{\alpha\gamma^2 n P_n(\zeta_2 r)}{r}\right], \quad a \leqslant r \leqslant b \tag{8d}$$

TABLE I
COMBINATIONS OF ξ_1, ζ_2, AND γ

Case No.	ξ_1	ζ_2	γ	Comments
1	Real	Real	Real	Not Permissible
2	Real	Real	Imaginary	Permissible for $k_1^2 > k_2^2$. Propagation in z-direction, trapped wave in r-direction.
3	Real	Imaginary	Real	Permissible. Cut-off wave in z-direction standing wave in r-direction. Replace I_n by J_n and K_n by Y_n in Eq. (8)-(14).
4	Real	Imaginary	Imaginary	Permissible. Propation in z-direction, standing wave in r-direction. Replace I_n by J_n and K_n by Y_n in Eq. (8)-(14).
5	Imaginary	Real	Real	Not permissible.
6	Imaginary	Real	Imaginary	Permissible. Propagation in z-direction, trapped wave in r-direction. Replace J_n by I_n in Eq. (8)-(14).
7	Imaginary	Imaginary	Real	Not permissible.
8	Imaginary	Imaginary	Imaginary	Permissible for $k_2^2 > k_1^2$. Propagation in z-direction, standing wave in r-direction. Replace J_n by I_n; I_n by J_n and K_n by Y_n in Eq. (8) - (14).

where A is an arbitrary constant, and where

$$\xi_1^2 = k_1^2 + \gamma^2 \quad \zeta_2^2 = -\left(k_2^2 + \gamma^2\right)$$

$$k_1^2 = \epsilon_{r_1} k_0^2 \quad k_2^2 = \epsilon_{r_2} k_0^2 \quad k_0^2 = \omega^2\mu_0\epsilon_0 \tag{9}$$

$$P_n(\zeta_2 r) = J_n(\xi_1 a)\left[\frac{K_n(\zeta_2 r)I_n'(\zeta_2 b) - I_n(\zeta_2 r)K_n'(\zeta_2 b)}{K_n(\zeta_2 a)J_n'(\zeta_2 b) - I_n(\zeta_2 a)K_n'(\zeta_2 b)}\right] \tag{10}$$

$$R_n(\zeta_2 r) = J_n(\xi_1 a)\left[\frac{K_n(\zeta_2 r)I_n(\zeta_2 b) - I_n(\zeta_2 r)K_n(\zeta_2 b)}{K_n(\zeta_2 a)I_n(\zeta_2 b) - I_n(\zeta_2 a)K_n(\zeta_2 b)}\right]$$

$$U_n = nJ_n(\xi_1 a)\left[\frac{1}{\xi_1^2 a^2} + \frac{1}{\zeta_2^2 a^2}\right] \tag{11}$$

$$V_n = \frac{J_n'(\xi_1 a)}{\xi_1 a} + \frac{P_n'(\zeta_2 a)}{\zeta_2 a}$$

$$\alpha = -\frac{U_n}{V_n}. \tag{12}$$

$J_n(\cdot)$, $I_n(\cdot)$, and $K_n(\cdot)$ are the Bessel functions and the modified Bessel functions of the first and second kinds, respectively. The propagation constant γ must be computed by solving the characteristic equation

$$U_n^2 a^2\gamma^2 + k_0^2 a^2 V_n W_n = 0 \tag{13}$$

where

$$W_n = \epsilon_{r_1}\frac{J_n'(\xi_1 a)}{\xi_1 a} + \epsilon_{r_2}\frac{R_n'(\zeta_2 a)}{\zeta_2 a}. \tag{14}$$

The field components and characteristic equation of (8) and (13) are based on the assumptions that the waves existing in the waveguide have real radial wavenumbers ξ_1

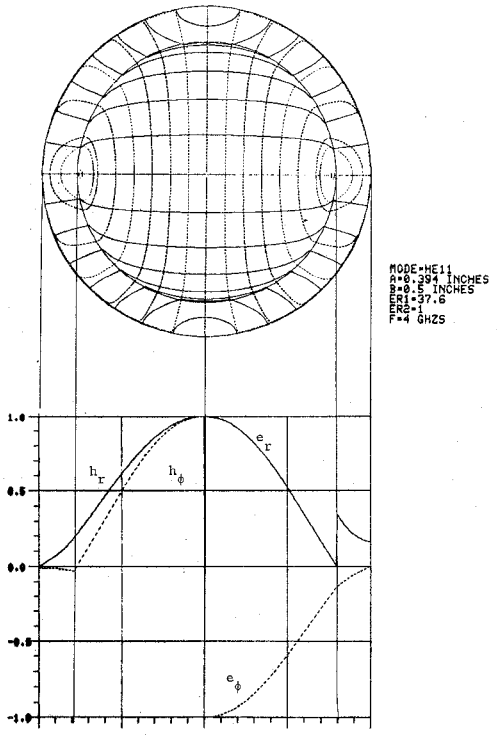

Fig. 3. Field distribution for HE_{11} mode.

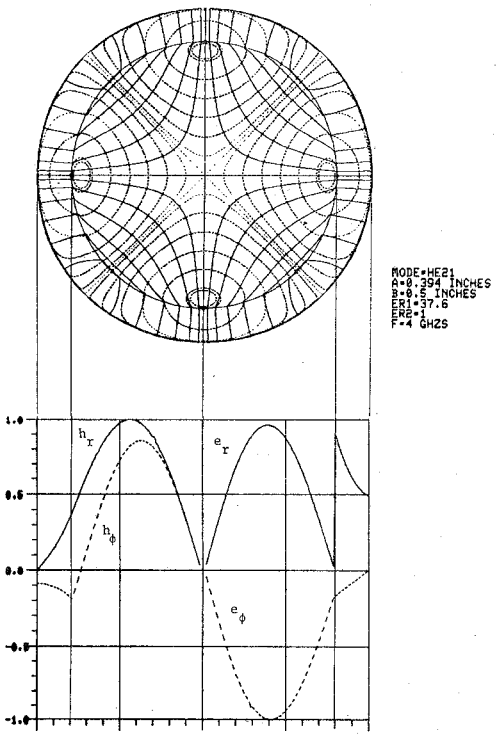

Fig. 5. Field distribution for HE_{21} mode.

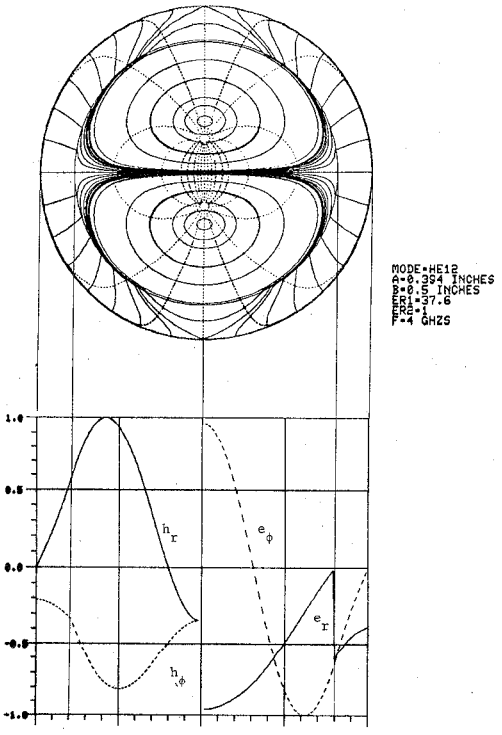

Fig. 4. Field distribution for HE_{12} mode.

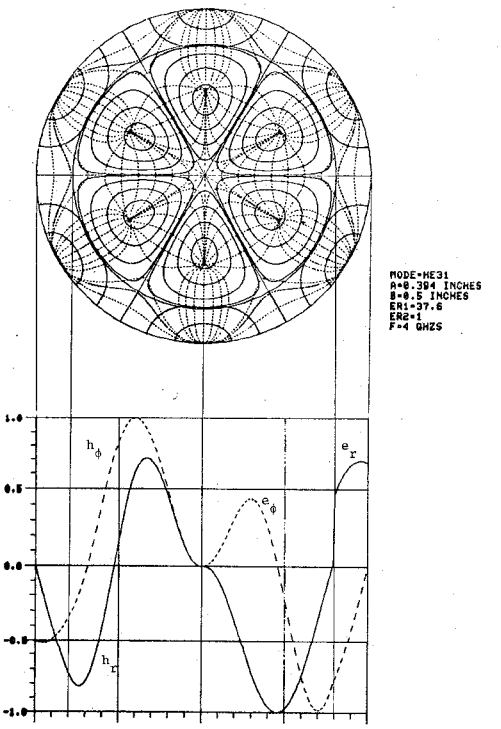

Fig. 6. Field distribution for HE_{31} mode.

and ζ_2. This assumption leads to the particular choices made for the radial functions (J_n for $r < a$, K_n and I_n for $r > a$) with real arguments. Several other types of solutions may exist, for which valid field configurations are possible. These possibilities are determined by the various combinations of the real and purely imaginary nature of the radial wavenumbers ξ_1, ζ_2 and the propagation constant γ. Table I shows all eight possible combinations that can be obtained by allowing each of the quantities ξ_1, ζ_2, and γ to take on either real or imaginary values. Valid combinations must satisfy (9) and (13) simultaneously. It is easily seen that combinations 1, 5, and 7 in Table I cannot satisfy these conditions, and hence are not permissible. The remaining five combinations can satisfy (9); however, the

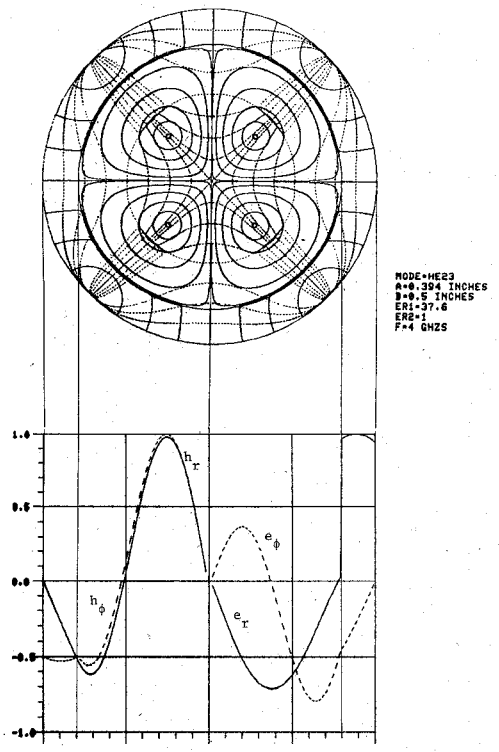

Fig. 7. Field distribution for HE_{23} mode.

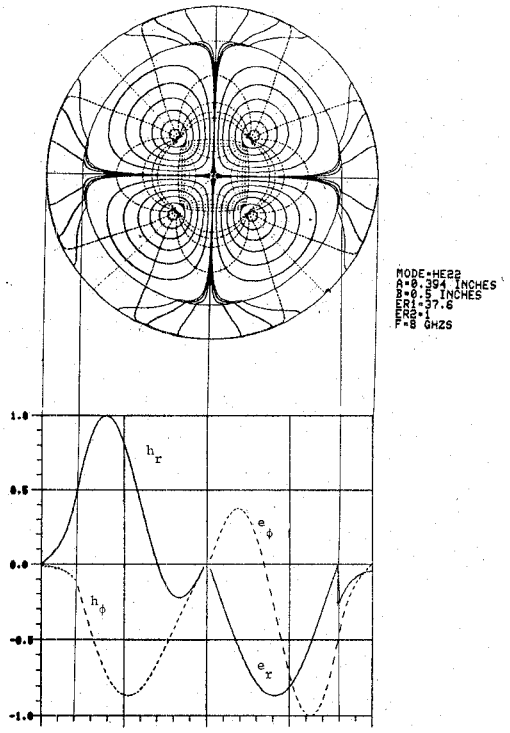

Fig. 9. Field distribution for HE_{22} mode.

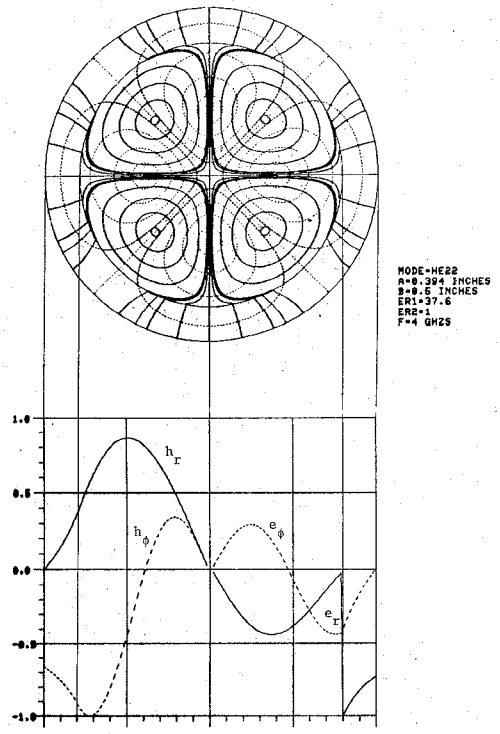

Fig. 8. Field distribution for HE_{22} mode.

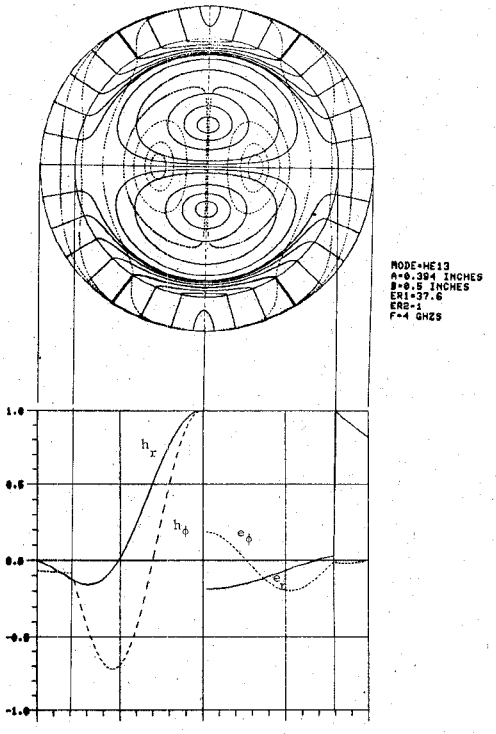

Fig. 10. Field distribution for HE_{13} mode.

existence of solutions must be determined for each of these combinations by finding if the roots of (13) exist. For the cases considered in this paper, no roots of (13) were found which correspond to ξ_1 being imaginary; hence, only combinations 2, 3, and 4 in Table I are considered.

Thus, for efficient numerical evaluation of the fields, rather than computing two two-dimensional arrays for E_r and E_ϕ from (6) and (7) at a grid of points (r_i, ϕ_i), only two one-dimensional arrays of values of the functions $e_r(r)$ and $e_\phi(r)$ given by (8) are computed and stored for a prescribed set of points (r_i) of the variable r. These values can subsequently be used with (2) and (3) to find the fields at any given location in the dielectric-loaded waveguide cross section. The increment in r_i can be chosen small

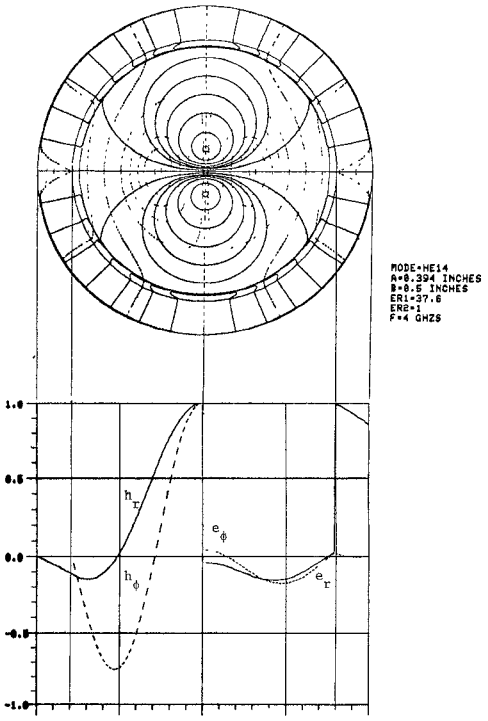

Fig. 11. Field distribution for HE_{14} mode.

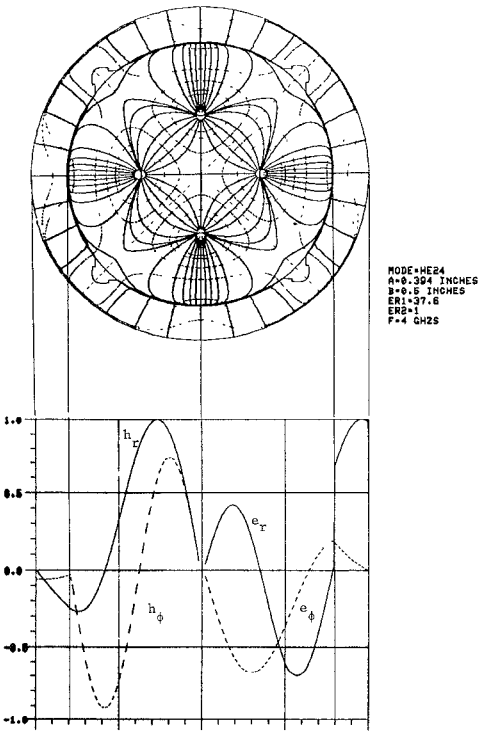

Fig. 12. Field distribution for HE_{24} mode.

enough so that, if necessary, linear interpolation can be used to find the values of the functions e_r and e_ϕ at intermediate points.

III. Field Plots—Results

Two sets of graphs are generated. The first set are field plots which display the direction of the transverse electric and magnetic field lines in the cross section of the guide.

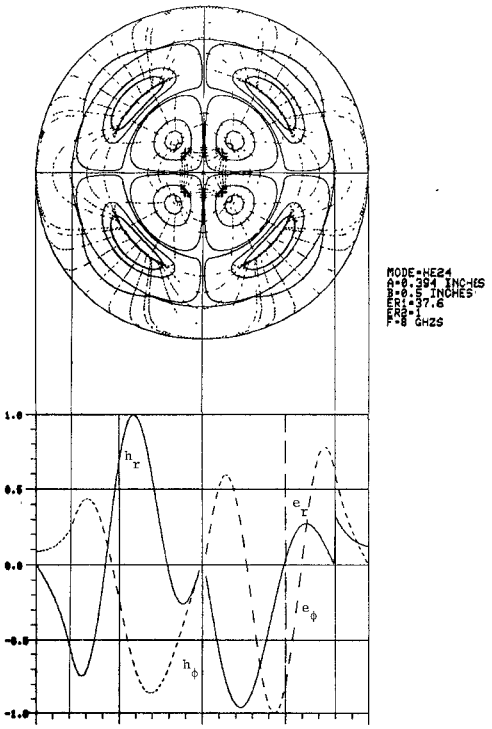

Fig. 13. Field distribution for HE_{24} mode.

TABLE II
Parameters of the Field Plots in Figs. 3–13

Figure No.	Mode	Frequency (GHz)	$(\xi_1 a)$	$(\xi_2 a)^2$	$(\beta a)^2$	α
3	HE_{11}	4.0	2.2607	20.6160	21.3190	0.7165
4	HE_{12}	4.0	4.4052	6.3203	7.0232	-5.5122
5	HE_{21}	4.0	3.6865	12.1360	12.8390	0.8038
6	HE_{31}	4.0	6.7953	-20.4500	-19.7480	-5.4173
7	HE_{23}	4.0	5.8560	-8.5659	-7.8630	-3.7744
8	HE_{22}	4.0	5.0922	-0.2040	0.4990	-21.5167
9	HE_{22}	8.0	5.9195	67.8650	70.6770	-2.7153
10	HE_{13}	4.0	5.2145	-1.4651	-0.7622	-5.2189
11	HE_{14}	4.0	5.3523	-2.9207	-2.2178	-1.2705
12	HE_{24}	4.0	6.6960	-19.1100	-18.4070	-0.1220
13	HE_{24}	8.0	8.8759	24.1240	26.9350	-7.8145

The second set show the variation of the field intensity in the radial direction by plotting the field components e_r, e_ϕ, h_r, and h_ϕ given by (8) as a function of r. Both sets are shown for the nine hybrid modes having the lowest cutoff frequencies, in Figs. 3–13. The parameters used in the generation of these plots are

$$\epsilon_{r_1} = 37.6 \quad b = 0.5'' \quad a = 0.396''.$$

Table II lists the rest of the relevant parameters for each of these figures. It should be noted that the modes with negative values of $(\beta a)^2$ are cutoff modes at the frequencies indicated. Figs. 3–5, 9, and 13 correspond to combination (2) in Table I; Figs. 6, 7, and 10–12, correspond to combination (4) in Table I, and Fig. 8 corresponds to combination (3) in Table I.

IV. Conclusions

The field plots presented in this paper are useful qualitative tools that display pictorially the field structures for the hybrid modes in dielectric-loaded waveguides. They can help in the design of devices using these modes by indicating locations of strong fields, their directions, etc. Mode types that can exist in the guiding structure are categorized in terms of possible combinations of propagating or cutoff waves in the axial direction, and standing or attenuating waves in the radial direction. Although the results were illustrated for a material of high dielectric constant and the frequency range 4–8 GHz, the technique and the programs developed are applicable for other materials and frequencies, including millimeter and optical wavelengths.

References

[1] K. A. Zaki and A. E. Atia, "Modes in dielectric-loaded waveguides and resonators," *IEEE Trans. Microwave Theory Tech.*, vol. MTT-31, pp. 1039–1045, Dec. 1983.

[2] A. S. Omar and A. K. Schunemann, "Scattering by dielectric obstacles inside guiding structures," in *1984 IEEE MTT-S Int. Microwave Symp. Dig.*, pp. 321–323, June 1984.

[3] Y. Kobayashi and S. Tanaka, "Resonant modes of a dielectric rod resonator short circuited at both ends by parallel conducting plates," *IEEE Trans. Microwave Theory Tech.*, vol. MTT-28, pp. 1077–1085, Oct. 1980.

[4] Y. Kobayashi and M. Miura, "Optimum design of shielded dielectric rod and ring resonators for obtaining the best mode separation," in *1984 IEEE MTT-S Int. Microwave Symp. Dig.*, pp. 184–186, June 1984.

[5] S. Maj and M. Pospieszalski, "A composite cylindrical dielectric resonator," in *1984 IEEE MTT-S Int. Microwave Symp. Dig.*, June 1984, pp. 190–192.

[6] D. Kajfez, A. V. Glisson, and J. James, "Computed modal field distribution of isolated dielectric resonators," in *1984 IEEE MTT-S Int. Microwave Symp. Dig.*, pp. 193–195, June 1984.

[7] P. E. Moller and R. H. Macphie, "On the graphical representation of electric field lines in waveguide," *IEEE Trans. Microwave Theory Tech.*, vol. MTT-33, pp. 187–192, Mar. 1985.

[8] E. R. Nagelberg and J. M. Hoffspiegel, "Computer-graphic analysis of dielectric waveguides," *IEEE Trans. Microwave Theory Tech.*, vol. MTT-15, pp. 187–189, Mar. 1967.

Kawthar A. Zaki (SM'85) received the B.S. degree with honors from Ain Shams University, Cairo, Egypt, in 1962, and the M.S. and Ph.D. degrees from the University of California, Berkeley, in 1966 and 1969, respectively, all in electrical engineering

From 1962 to 1964, she was a Lecturer in the Department of Electrical Engineering, Ain Shams University. From 1965 to 1969, she held the position of Research Assistant in the Electronic Research Laboratory, University of California, Berkeley. She joined the Electrical Engineering Department, University of Maryland, College Park, MD, in 1970, where she is presently an Associate Professor. Her research interests are in the areas of electromagnetics, microwave circuits, optimization, and computer-aided design.

Dr. Zaki is a member of Tau Beta Pi.

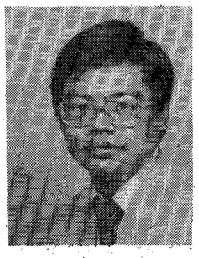

Chunming Chen (S'85) was born in Taiwan, Republic of China, in 1958. He received the B.S. degree from the National Tsing Hua University, Taiwan, in 1981, and the M.S. degree from the University of Maryland, College Park, in 1985, both in electrical engineering.

Since 1984, he has worked as a Research Assistant in the Department of Electrical Engineering, University of Maryland, College Park. He is now working towards a Ph.D. degree in the area of microwave components and circuits.